Journal of Materials Chemistry B

RSC Publishing

PAPER

View Article Online
View Journal | View Issue

Cite this: J. Mater. Chem. B, 2013, 1, 6525

One-pot green synthesis, characterizations, and biosensor application of self-assembled reduced graphene oxide–gold nanoparticle hybrid membranes

Panpan Zhang,[a] Xiaoyuan Zhang,[a] Siyu Zhang,[a] Xin Lu,[a] Qing Li,[b] Zhiqiang Su*[a] and Gang Wei*[b]

We report here a facile one-pot green synthesis method to prepare a self-assembled membrane of reduced graphene oxide–gold nanoparticle (RGO–AuNP) nanohybrids at a liquid–air interface. The obtained sandwich-like multilayer RGO–AuNP hybrid membranes were characterized by atomic force microscopy, scanning electron microscopy, transmission electron microscopy, UV-vis spectroscopy, Fourier transform infrared spectroscopy, X-ray diffraction, and Raman spectroscopy, and the obtained results prove that GO and chloroauric acid ($HAuCl_4$) were synchronously reduced by glucose successfully. In addition, the experimental data indicate that the self-assembly and formation of RGO–AuNP hybrid membranes are mainly governed by the Brownian motion and electrostatic interaction between RGO and AuNPs, and the encapsulation of AuNPs in the hybrid membrane can be easily adjusted by changing the concentration of $HAuCl_4$. The created functional semi-transparent RGO–AuNP hybrid membranes are very stable in various organic and inorganic solvents, and can be used to fabricate a novel nonenzymatic amperometric biosensor of hydrogen peroxide (H_2O_2). The fabricated H_2O_2 biosensor reveals a wide linear range from 0.25 to 22.5 mM, low detection limit of 6.2 μM ($S/N = 3$), high selectivity, and long-term stability. It is expected that this one-pot green method for fabricating sandwich-like multilayer hybrid functional membranes has broad applications in biosensing, catalysis, and energy storage.

Received 16th September 2013
Accepted 16th October 2013

DOI: 10.1039/c3tb21270j

www.rsc.org/MaterialsB

1. Introduction

Graphene as a popular one-atom-thick two-dimensional (2-D) sheet with hexagonal honeycomb lattices has been widely used in nanotechnology,[1,2] materials science,[3,4] and biotechnology.[5–7] In recent years, much interest has been focused on the hybridization of graphene with various organic and inorganic nanomaterials to create functional nanohybrids and even the hybrid membranes.[8–12] For example, Wu *et al.* reported the preparation of flexible graphene–polyaniline nanofiber composite films and their application in supercapacitor devices,[11] and they found that the prepared composite films exhibit improved electrochemical stability and rate performances. Meanwhile, Yu *et al.* prepared free-standing layer-by-layer assembled hybrid graphene–MnO_2 nanotube (NT) thin films by an ultrafiltration technique and utilized them as anodes with porous structures for lithium ion batteries.[12] Hybrid membranes, compared to bulk materials, have the advantages of low cost, large area, light weight and easy preparation. In addition to that, the graphene-based hybrid membranes or films are also found to have improved electrical, catalytic, chemical, and mechanical performances.[13–16] Previously, Chen *et al.* utilized a simple filtration method to create highly conductive and flexible papers composed of graphene sheets and 1D silver nanowires.[15] Borowiec *et al.* decorated nitrogen-doped graphene nanosheets with gold nanoparticles (AuNPs) as an improved sensor for electrochemical determination of chloramphenicol.[16] So far, graphene-based hybrid membranes have been widely studied and applied in catalysis,[17] sensing,[18] surface enhanced detection,[19,20] and energy storage.[21]

Typically, two strategies have been utilized to fabricate graphene–metallic nanoparticle (MNP) hybrid membranes. In the first strategy, hybrid membranes were prepared by first producing the GO nanosheets, then modifying the GO nanosheets with prepared MNPs, and finally reducing the GO nanosheets.[22–28] For instance, Kong *et al.* produced layer-by-layer films comprised of alternating graphene and AuNPs by a two-step procedure,[25] which involves the use of vacuum filtration of a reduced graphene oxide (RGO) solution to fabricate thin graphene films on a quartz substrate, followed by creating AuNPs on the prepared graphene films. More recently, Kholmanov *et al.* reported the preparation of transparent and

[a]State Key Laboratory of Chemical Resource Engineering, Beijing University of Chemical Technology, 100029 Beijing, China. E-mail: suzq@mail.buct.edu.cn
[b]Hybrid Materials Interface Group, Faculty of Production Engineering, University of Bremen, D-28359 Bremen, Germany. E-mail: wei@uni-bremen.de; Fax: +49 421 218 64599

conductive RGO–MNP hybrid membranes by first spin-coating different metallic nanowires on a glass slide and then coating a GO/AuNP film on this substrate.[26–28] The final hybrid GO–MNP membrane was reduced to RGO–MNP by exposing it to hydrazine vapor at 100 °C for 24 h. Highly reduced GO hybrid membranes have excellent electrical properties, but the fabrication processes are very tedious and complicated. In the other strategy there are some improvements that involve synchronous reduction of GO and metallic ions in one system.[29–35] For instance, Hassan and co-workers utilized microwave synthesis to synchronously reduce GO aqueous dispersions and a variety of metal salts in the presence of various reducing agents like ethylenediamine or ammonium hydroxide.[31] It is worth noting that in both strategies the RGO–MNP hybrid membranes were fabricated by complicated processes, such as vacuum filtration, spin-coating, spray deposition and chemical vapour deposition.[32–35] Moreover, the reducing agents used in these strategies, such as hydrazine hydrate, sodium borohydride and hydrohalic acids, are toxic and harsh, and the fabrication of graphene-based membranes is very complicated.

In this work, we demonstrate a facile one-pot green synthesis strategy for the successful preparation of large-scale and semi-transparent RGO–AuNP hybrid membranes. For the first time, we utilized glucose to reduce GO and $HAuCl_4$ in one liquid system synchronously and finally we fabricated RGO–AuNP hybrid membranes at a liquid–air interface by a self-assembly process. Furthermore, we investigated the structure and properties of the prepared RGO–AuNP hybrid membranes and explored their potential application in fabricating an electrochemical biosensor of hydrogen peroxide (H_2O_2).

2. Experimental section

2.1 Reagents and materials

Natural graphite flake (99.8% purity), chloroauric acid ($HAuCl_4 \cdot 3H_2O$, ≥49.0% Au basis), sodium citrate tribasic dehydrate (≥99.0% purity), and Nafion solution (~5% in a mixture of lower aliphatic alcohols and water) were purchased from Sigma-Aldrich. Ascorbic acid (AA), uric acid (UA), dopamine (DA) and glucose were obtained from J&K Scientific Ltd. (Beijing, China). Na_2HPO_4, NaH_2PO_4, phosphoric acid, sulfuric acid, hydrochloric acid, potassium permanganate ($KMnO_4$), ethanol, *N*-dimethylformamide (DMF), and diethyl ether were purchased from Beijing Chemicals Co., Ltd. (Beijing, China). H_2O_2 (analytical grade, 30% aqueous solution) was supplied by Tianjin Dongfang Chemical Plant (Tianjin, China). All chemicals used in this work were of analytical reagent grade and obtained from commercial sources and directly used without additional purification. The water used was purified through a Millipore system (~18.2 MΩ cm). Carbon-coated Cu grids for transmission electron microscopy (TEM) characterization were purchased from Plano GmbH (Wetzlar, Germany).

2.2 Preparation of the RGO–AuNP hybrid membrane

Fig. 1 shows the schematic model of the one-pot green synthesis of the RGO–AuNP hybrid membrane. For the preparation of

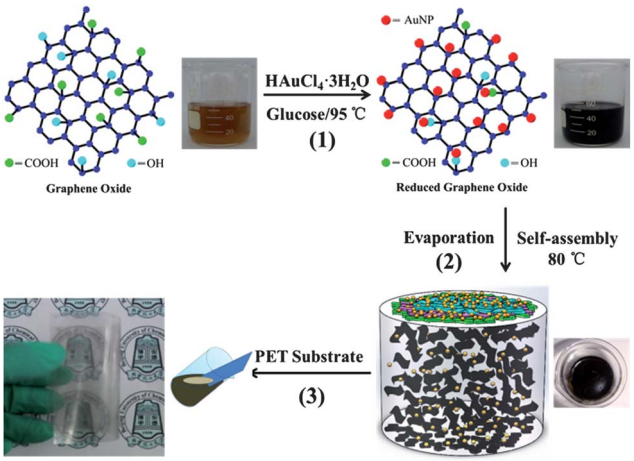

Fig. 1 Schematic presentation of the one-pot green synthesis of the self-assembled RGO–AuNP hybrid membrane.

starting materials, graphite oxide was prepared from natural graphite flake by using the modified Hummers method.[36] To yield the exfoliation of a GO (0.5 mg mL^{-1}) aqueous dispersion, sonication was carried out with a bath sonicator (100 W, 40 kHz) for 1 hour. First, GO (50 mL) and $HAuCl_4$ (25 μL, 507.83 mM) in aqueous solution were mixed together and reduced to RGO and AuNPs by glucose (2.4 g) by heating at 95 °C (step 1). Then 200 μL of ammonia solution (30 wt% in water) was added into the mixture,[37,38] and the temperature was decreased to 80 °C. With the continuous evaporation at about 80 °C for 5 min, the formed RGO interacted with AuNPs and then self-assembled into a multilayer structure (step 2). Finally, a stable RGO–AuNP hybrid membrane was harvested from the suspension with a polyethylene terephthalate (PET) substrate (step 3). The prepared RGO–AuNP hybrid membrane was stable, flexible, and semi-transparent, with an adjustable size.

2.3 Stability test of RGO–AuNP hybrid membranes

In order to evaluate the stability of RGO–AuNP hybrid membranes, hybrid membranes were immersed into different organic agents for different times at room temperature. Water, PBS (0.1 M, pH = 7.6), ethanol, and DMF were chosen because they are commonly used solvents. Four flakes of RGO–AuNP hybrid membranes were immersed into these four agents for 0, 4, 8, and 12 hours, respectively.

2.4 Preparation, characterization of RGO-, AuNP- and RGO–AuNP hybrid membrane-modified electrodes

The glassy carbon electrode (GCE, 3.0 mm in diameter) was polished with 1 and 0.3 μm alumina slurry, and then successively washed with distilled water in an ultrasonic bath. For the preparation of the RGO- (or AuNP-) modified GCE, 10 mg RGO (or 100 μL AuNP solution), 1 mL ethanol, and 100 μL Nafion (0.1%) were mixed in an ultrasonic bath for 15 min. Then 10 μL of this mixture suspension was dropped onto the pre-treated GCE and dried in air. The RGO–AuNP modified GCE was made by directly transferring the hybrid membrane onto the surface

of the GCE. Such modified electrodes were used for the CV and amperometric response experiments.

2.5 Experimental techniques

AFM images were recorded using a NanoWizard 3 NanoScience atomic force microscope (JPK Instruments AG, Germany) in tapping mode. SEM experiments were performed on a JSM-6700F scanning electron microscope (JEOL). The sample surface was deposited on a Pt layer to protect the surface layers from ion beam damage. A large trench was milled at 10.0 kV and an ion beam current of 12 pA. TEM experiments were performed on a Tecnai $G^2$20 transmission electron microscope (FEI) with an accelerating voltage of 200 kV, and samples were prepared by transferring the RGO–AuNP hybrid membrane onto the copper grid, and dried at room temperature. UV-visible spectroscopy (UV-2900, Hitachi, Japan, scanning rate 400 nm min^{-1}), Fourier transform infrared spectroscopy (FTIR, Nicolet 6700, Thermo-Fisher, USA), X-ray diffraction (XRD, Rigaku D/max-2500 VB+/PC), and Raman spectroscopy (LabRAM HORIBA JY, Edison, NJ) were used to compare the structures of the GO with RGO–AuNP hybrid membranes.

All the electrochemical experiments were carried out using an electrochemical workstation (CHI760D, Chenhua, Shanghai) at room temperature. A conventional three-electrode system was employed with a modified GCE as a working electrode, a Pt wire as an auxiliary electrode, and a KCl saturated calomel electrode (SCE) as a reference electrode. The test solution was phosphate buffer solutions (PBS, 0.1 M) with pH = 7.6, which were prepared with 0.1 M NaH_2PO_4 and 0.1 M Na_2HPO_4 and deoxygenated with highly pure nitrogen for 20 minutes before electrochemical experiments. All potentials in this work are referenced to the SCE. The curves of cyclic voltammograms (CVs) in this work were obtained after six scans under steady state conditions. Amperometric measurements were carried out under stirring conditions.

3. Results and discussion

3.1 Morphology and structure of the produced RGO–AuNP hybrid membrane

The morphology and structure of the produced RGO–AuNP hybrid membrane was observed by AFM, SEM, and TEM. Fig. 2a and b show a typical AFM height image of the hybrid membrane harvested on a silicon substrate. It can be found that this membrane is flat with a roughness of about 1.25 nm and some AuNPs are bound on the surface of the membrane. AFM section analysis indicates that the height of AuNPs is about 8 nm (Fig. 2c). The large-scale SEM image (Fig. 2d) indicates that the hybrid membrane is very smooth and its surface was covered by AuNPs uniformly. It should be noted that the hybrid membrane has a sandwich-like multilayer structure of RGO and AuNPs, and therefore the morphological characterization (AFM and SEM) can only see the AuNPs on the surface of the membrane but not the inner ones. In the next step, this RGO–AuNP hybrid membrane was harvested with a copper grid for TEM characterization. It is clear that the self-assembled RGO–AuNP hybrid membrane is uniform and decorated with dispersed AuNPs (Fig. 2e and f). Comparing the corresponding TEM images and SEM image of the hybrid membrane, it can be found that more AuNPs were observed and therefore our previous hypothesis of the sandwich-like structure on the created RGO–AuNP hybrid membrane was identified. With this one-pot green synthesis, the thickness of the RGO–AuNP hybrid membrane is controllable and reproducible by adjusting the concentration of RGO and AuNPs, the temperature and the evaporation period.

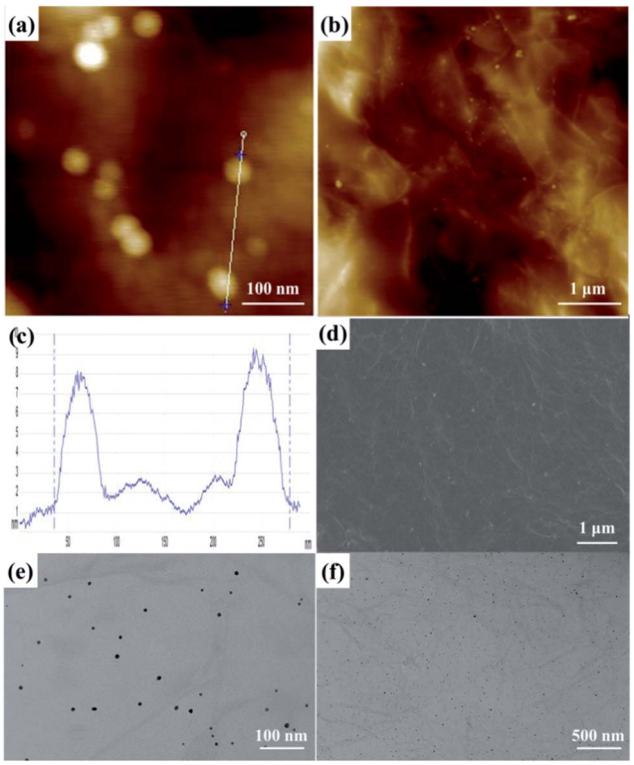

Fig. 2 Morphological and structural characterizations of the RGO–AuNP hybrid membrane: (a–c) AFM images and section analysis, (d) SEM, and (e and f) TEM.

A control experiment indicates that the encapsulation of AuNPs in the hybrid membrane can be adjusted by changing the concentration of $HAuCl_4$. Fig. 3 shows the typical TEM images with different encapsulations of AuNPs in the RGO–AuNP hybrid membranes. AuNPs with a uniform size (~8 nm) are clearly seen in the hybrid membranes for all the samples. These samples are prepared by adjusting the dosage of $AuCl_4^-$ ions, and the different dosages are 10, 15, 20, and 25 μL of $HAuCl_4$ (507.83 mM).

The optical transmittance of the harvested RGO–AuNP hybrid membrane was measured by UV-vis spectroscopy, and the results are shown in Fig. 4a. It can be found that there is a sharp decrease of transmittance from 300 to 320 nm, which means that the prepared membrane prevents UV light (10–400 nm) from being transmitted. Meanwhile, the optical transmittance increases sharply with the wavelength in the visible region (390–700 nm) and retains a high value of about 87% in the near-infrared (above 800 nm) region, proving its semi-transparent properties.

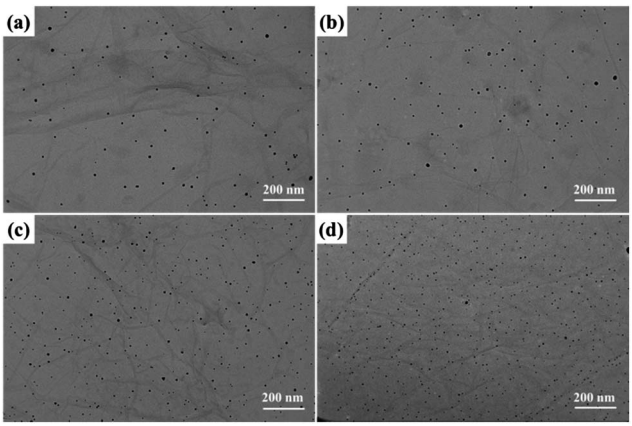

Fig. 3 TEM images of RGO–AuNP hybrid membranes with different AuNP encapsulations.

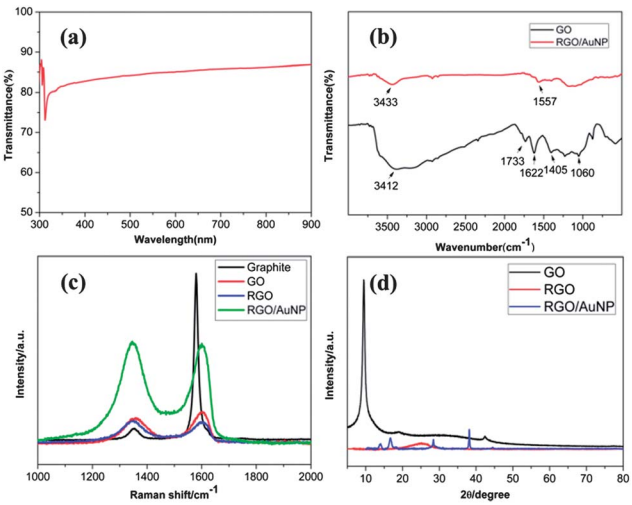

Fig. 4 Property and structure characterization of GO, RGO and RGO–AuNP hybrid membrane: (a) optical transmittance, (b) FTIR spectra, (c) Raman spectra, and (d) XRD patterns.

The structural variation of GO before and after reduction was further detected by Fourier transform infrared spectroscopy (FT-IR), X-ray diffraction (XRD) and Raman spectroscopy. Fig. 4b presents the FT-IR spectra of GO and RGO–AuNP hybrid membrane. The spectrum of GO shows several absorption peaks at 3412 and 1405 cm^{-1} (ν_{O-H}), 1733 cm^{-1} (C═O stretching), 1622 cm^{-1} ($\nu_{C=C}$), and 1060 cm^{-1} (ν_{C-O}).[39] For the reduced hybrid membrane, the characteristic absorption peaks of oxide groups (ν_{O-H}, $\nu_{C=O}$, and ν_{C-O}) were found to decrease dramatically, indicating that the GO has been reduced to the RGO. Fig. 4c presents the Raman spectra of the RGO–AuNP hybrid membrane and three related samples. The G-band of GO is broadened and up-shifted compared with that of graphite (1575 cm^{-1}), which can be attributed to the presence of isolated double bonds.[40] Moreover, the D-band of GO at 1356 cm^{-1} becomes prominent compared with that of graphite, which indicates that the reduction in the size of the in-plane sp^2 domains is ascribed to the extensive oxidation. After reduction, the G- and D-bands of RGO and RGO–AuNP membrane are located at 1605 and 1350 cm^{-1}, corresponding to the recovery of the hexagonal defected carbon atom network. In addition, the I_D/I_G of RGO and RGO–AuNP membrane increasing from 0.77 to 1.03 indicates the reduction of GO to RGO.[41] Power XRD was further used to characterize GO, RGO and RGO–AuNP membrane, and the typical patterns are shown in Fig. 4d. A typical narrow peak at 9.48° (d-spacing ~ 9.32 Å) was observed in the XRD pattern of GO, but the peak of RGO shows a dramatic shift to higher 2θ angles (25.13°; d-spacing ~ 3.54 Å), which suggests that RGO is well ordered two-dimensional sheets and has smaller average interlayer spacing.[42]

3.2 Potential formation mechanism of the RGO–AuNP membrane

Based on the above results, we proposed a potential formation mechanism of the RGO–AuNP hybrid membrane (Fig. 5). After mixing $AuCl_4^-$ ions with GO by vigorous stirring for several minutes, the $AuCl_4^-$ ions and GO sheets disperse uniformly. During heating, the mixed GO and $AuCl_4^-$ dispersion was reduced by glucose and transformed into RGO and AuNPs, respectively. Through Brownian motion and electrostatic interaction, AuNPs tend to attach to the defects and residual oxygen-containing groups of RGO sheets.[43,44] Moreover, the liquid level of the mixed dispersion was gradually decreased with the solvent evaporation, increasing the possibility of collision and interaction between free AuNPs and RGO sheets. With the help of Brownian motion, both the RGO and AuNPs can easily move to the liquid–air interface.[45] The liquid–air interface provides a smooth space for the interaction and self-assembly between AuNPs and 2-D RGO.

In a previous report, Kholmanov and coworkers reported that the RGO/copper nanowire hybrid films fabricated by spin coating have high-performance as electrochemical electrodes.[27] We expected that the combination of RGO and AuNP will improve the conductivity and catalysis of the fabricated hybrid membrane, which will have better performance compared to both RGO and AuNPs. Before electrochemical experiments, we first checked the stability of the produced RGO–AuNP hybrid membranes in water, PBS, ethanol, and *N*-dimethylformamide. Four flakes of hybrid membranes were immersed into the solvents for different periods, and it is clear that the membranes have no significant changes after 12 hours (Fig. 6),

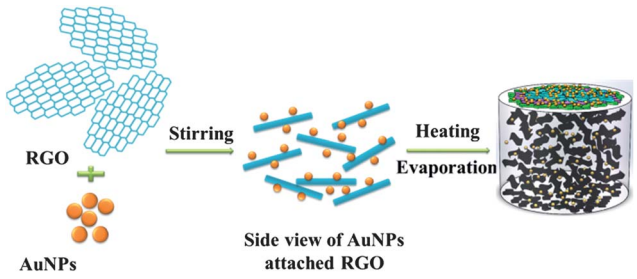

Fig. 5 Schematic presentation of the potential formation mechanism of the RGO–AuNP hybrid membrane.

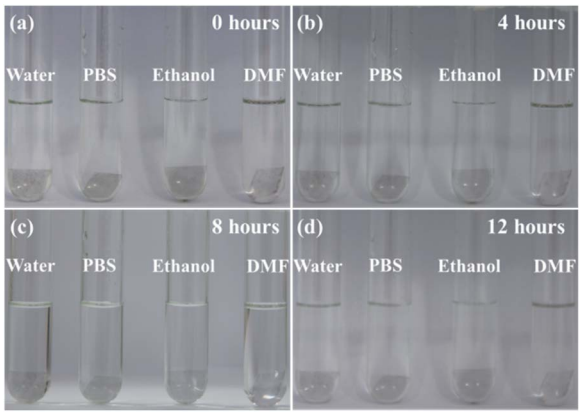

Fig. 6 Optical photographs of RGO–AuNP hybrid membranes in four solvents for different periods.

which proves the high stability of our membranes. In the next step, we investigated the synthesized RGO–AuNP hybrid membrane as a novel material for fabricating an electrochemical H_2O_2 biosensor. A glass carbon electrode (GCE) was polished and covered with the formed RGO–AuNP hybrid membrane for the subsequent H_2O_2 catalysis and sensing.

3.3 Potential application in sensing of H_2O_2

Fig. 7a shows the cyclic voltammograms (CVs) of RGO-, AuNP- and RGO–AuNP hybrid membrane-modified GCEs in the presence of 15 mM H_2O_2. The RGO-modified GCE shows no apparent redox processes and the AuNP-modified GCE shows a very small current response and a broad reduction peak from about −0.4 to −0.2 V. The hybrid membrane-modified GCE shows a reduction peak at about −0.294 V and an obvious positive shift of both the onset potential and current peak compared to GO- and AuNP-modified GCEs.[46] Herein, −0.294 V was selected as the applied potential for *I–T* measurements.

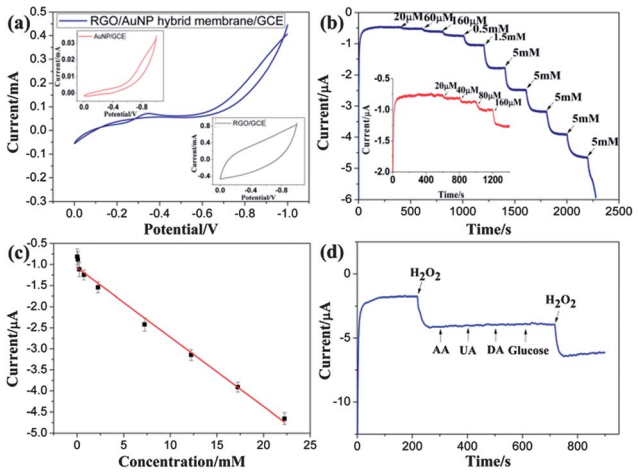

Fig. 7 Electrochemical biosensing: (a) CVs of GCEs modified with RGO, AuNPs, and RGO–AuNP membrane. (b) *I–T* response of the RGO–AuNP membrane-modified GCE in 0.1 M PBS with successive addition of H_2O_2 at −0.294 V *vs.* SCE. (c) Calibrated line. (d) Selectivity of the biosensor.

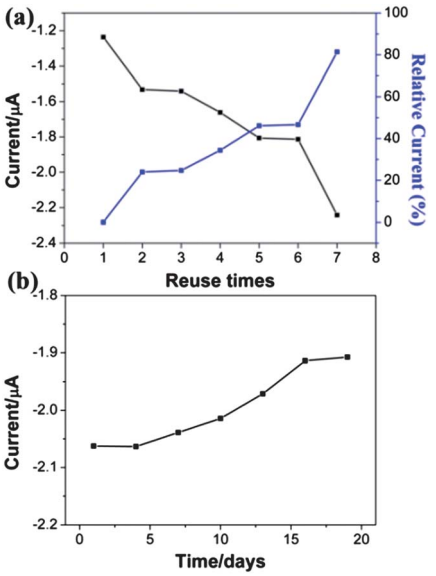

Fig. 8 (a) Reusability and (b) long-term storage stability in response to 5 mM H_2O_2.

Fig. 7b shows a stable response over the long period test and rapid increase in the cathodic current as a result of the reduction of H_2O_2 upon the addition of H_2O_2 solution. The calibration curve (Fig. 7c) indicates a linear response to H_2O_2 and the linear range of the H_2O_2 detection is from 0.25 to 22.5 mM ($R = 0.9894$, $S/N = 3$), the limit of detection (LOD) is calculated to be 6.2 μM ($S/N = 3$) with a sensitivity of 5.3 μA mM^{-1} cm^{-2}. The selectivity test is demonstrated in Fig. 7d, which compares the amperometric response for four relevant electroactive species, such as ascorbic acid (AA), uric acid (UA), dopamine (DA), and glucose. No interference was observed at a potential of −0.294 V, indicating the high selectivity toward the detection of H_2O_2.

The reuse stability of the RGO–AuNP hybrid membrane-modified GCE is also shown in Fig. 8a, indicating that the repeated usage of the created biosensor is possible, at least 6 times. Significant reduction in current after 6 times of use is depicted, which was ascribed to the detachment of the membrane from the electrode. Furthermore, the electrostatic interaction and Brownian motion between RGO sheets and AuNPs are strengthened during the heating process.

The long-term stability of the RGO–AuNP hybrid membrane-modified GCE was explored over a 15 day period (Fig. 8b). The fabricated sensor was stored in a refrigerator at 4 °C and measured every 2–4 days. The result shows that the catalytic current response retains more than 92.5% of its initial value in response to 5 mM H_2O_2 after 15 days, indicating an acceptable stability of the modified electrode.

4. Conclusions

In summary, we have demonstrated a facile one-pot green synthesis of the RGO–AuNP hybrid membrane and investigated the potential application of this hybrid membrane as a biosensor material. Governed by the Brownian motion, the

RGO–AuNP hybrid membranes were formed through a self-assembly process at the liquid–air interface. Compared to previous reports, our strategy for producing RGO-based hybrid membranes has several advantages, such as environmental friendliness, time saving, high efficiency, and cost-effectiveness. Electrochemical data indicate that the RGO–AuNP hybrid membrane exhibits good electrocatalytic activity toward H_2O_2 and the prepared H_2O_2 biosensor based on this hybrid membrane shows a wide linear range, low detection limit, high selectivity and long-term stability. We expect this one-pot green synthesis method can be utilized to prepare other functional materials based on RGO and MNPs. Other potential applications of the produced RGO–AuNP hybrid membranes in catalysis, surface-enhanced Raman scattering and energy storage are under study in our laboratory.

Acknowledgements

The authors gratefully acknowledge the financial support from the Beijing New-Star Program of Science and Technology (2009B10), and the Fundamental Research Funds for the Central Universities (project no. ZZ1307). We would like to thank the financial support of the China Scholarship Council (CSC) for a PhD scholarship in the University of Bremen.

Notes and references

1 A. K. Geim and K. S. Novoselov, *Nat. Mater.*, 2007, **6**, 183.
2 V. Georgakilas, M. Otyepka, A. B. Bourlinos, V. Chandra, N. Kim, K. C. Kemp, P. Hobza, R. Zboril and K. S. Kim, *Chem. Rev.*, 2012, **112**, 6156.
3 M. Quintana, E. Vazquez and M. Prato, *Acc. Chem. Res.*, 2013, **46**, 138.
4 H. Xu and K. S. Suslick, *J. Am. Chem. Soc.*, 2011, **133**, 9148.
5 M. Yang, J. Yao and Y. Duan, *Analyst*, 2013, **138**, 72.
6 N. Mohanty and V. Berry, *Nano Lett.*, 2008, **8**, 4469.
7 S. He, K. K. Liu, S. Su, J. Yan, X. Mao, D. Wang, Y. He, L. J. Li, S. Song and C. Fan, *Anal. Chem.*, 2012, **84**, 4622.
8 S. Stankovich, D. A. Dikin, G. H. B. Dommett, K. M. Kohlhaas, E. J. Zimney, E. A. Stach, R. D. Piner, S. T. Nguyen and R. S. Ruoff, *Nature*, 2006, **442**, 282.
9 S. Bai and X. Shen, *RSC Adv.*, 2012, **2**, 64.
10 G. Wei, Y. Zhang, S. Steckbeck, Z. Su and Z. Li, *J. Mater. Chem.*, 2012, **22**, 17190.
11 Q. Wu, Y. Xu, Z. Yao, A. Liu and G. Shi, *ACS Nano*, 2010, **4**, 1963.
12 A. Yu, H. W. Park, A. Davies, D. C. Higgins, Z. Chen and X. Xiao, *J. Phys. Chem. Lett.*, 2011, **2**, 1855.
13 H. V. Rizo, I. M. Gullon and M. Terrones, *ACS Nano*, 2012, **6**, 4565.
14 J. Lin, Z. Peng, C. Xiang, G. Ruan, Z. Yan, D. Natelson and J. M. Tour, *ACS Nano*, 2013, **7**, 6001.
15 J. Chen, H. Bi, S. Sun, Y. Tang, W. Zhao, T. Lin, D. Wan, F. Huang, X. Zhou, X. Xie and M. Jiang, *ACS Appl. Mater. Interfaces*, 2013, **5**, 1408.
16 J. Borowiec, R. Wang, L. Zhu and J. Zhang, *Electrochim. Acta*, 2013, **99**, 138.
17 J. Yang, J. H. Yu, J. R. Strickler, W. J. Chang and S. Gunasekaran, *Biosens. Bioelectron.*, 2013, **47**, 530.
18 N. Liu, X. Chen and Z. Ma, *Biosens. Bioelectron.*, 2013, **48**, 33.
19 K. Jasuja and V. Berry, *ACS Nano*, 2009, **3**, 2358.
20 G. Lu, H. Li, C. Liusman, Z. Yin, S. Wu and H. Zhang, *Chem. Sci.*, 2011, **2**, 1817.
21 Y. Xu, Z. Lin, X. Huang, Y. Liu, Y. Huang and X. Duan, *ACS Nano*, 2013, **7**, 4042.
22 C. Xu, X. Wang and J. Zhu, *J. Phys. Chem. C*, 2008, **112**, 19841.
23 C. Nethravathi, E. A. Anumol, M. Rajamathi and N. Ravishankar, *Nanoscale*, 2011, **3**, 569.
24 R. Muszynski, B. Seger and P. V. Kamat, *J. Phys. Chem. C*, 2008, **112**, 5263.
25 B. S. Kong, J. Geng and H. T. Jung, *Chem. Commun.*, 2009, 2174.
26 I. N. Kholmanov, M. D. Stoller, J. Edgeworth, W. H. Lee, H. Li, J. Lee, C. Barnhart, J. R. Potts, R. Piner, D. Akinwande, J. E. Barrick and R. S. Ruoff, *ACS Nano*, 2012, **6**, 5157.
27 I. N. Kholmanov, S. H. Domingues, H. Chou, X. Wang, C. Tan, J. Y. Kim, H. Li, R. Piner, A. J. G. Zarbin and R. S. Ruoff, *ACS Nano*, 2013, **7**, 1811.
28 I. N. Kholmanov, C. W. Magnuson, A. E. Aliev, H. Li, B. Zhang, J. W. Suk, L. L. Zhang, E. Peng, S. H. Mousavi, A. B. Khanikaev, R. Piner, G. Shvets and R. S. Ruoff, *Nano Lett.*, 2012, **12**, 5679.
29 C. Tan, X. Huang and H. Zhang, *Mater. Today*, 2013, **16**, 29.
30 K. Vinodgopal, B. Neppolian, I. V. Lightcap, F. Grieser, M. Ashokkumar and P. V. Kamat, *J. Phys. Chem. Lett.*, 2010, **1**, 1987.
31 H. M. A. Hassan, V. Abdelsayed, A. E. R. S. Khder, K. M. AbouZeid, J. Terner, M. S. E. Shall, S. I. A. Resayes and A. A. E. Azhary, *J. Mater. Chem.*, 2009, **19**, 3832.
32 D. Wang, R. Kou, D. Choi, Z. Yang, Z. Nie, J. Li, L. V. Saraf, D. Hu, J. Zhang, G. L. Graff, J. Liu, M. A. Pope and I. A. Aksay, *ACS Nano*, 2010, **4**, 1587.
33 M. S. Lee, K. Lee, S. Y. Kim, H. Lee, J. Park, K. H. Choi, H. K. Kim, D. G. Kim, D. Y. Lee, S. W. Nam and J. U. Park, *Nano Lett.*, 2013, **13**, 2814.
34 M. Sawangphruk, P. Srimuk, P. Chiochan, A. Krittayavathananon, S. Luanwuthi and J. Limtrakul, *Carbon*, 2013, **60**, 109.
35 P. Mulpur, R. Podila, K. Lingam, S. K. Vemula, S. S. Ramamurthy, V. Kamisetti and A. M. Rao, *J. Phys. Chem. C*, 2013, **117**, 17205.
36 D. C. Marcano, D. V. Kosynkin, J. M. Berlin, A. Sinitskii, Z. Sun, A. Slesarev, L. B. Alemany, W. Lu and J. M. Tour, *ACS Nano*, 2010, **4**, 4806.
37 C. Zhu, S. Guo, Y. Fang and S. Dong, *ACS Nano*, 2010, **4**, 2429.
38 N. Wang, S. Xu and Y. Zhou, *Anal. Sci.*, 2007, **23**, 189.
39 I. K. Moon, J. Lee, R. S. Ruoff and H. Lee, *Nat. Commun.*, 2010, **1**, 73.
40 J. Zabel, R. R. Nair, A. Ott, T. Georgiou, A. K. Geim, K. S. Novoselov and C. Casiraghi, *Nano Lett.*, 2012, **12**, 617.

41 A. C. Ferrari and J. Robertson, *Phys. Rev. B: Condens. Matter Mater. Phys.*, 2000, **61**, 14095.
42 H. Yang, C. Shan, F. Li, D. Han, Q. Zhang and L. Niu, *Chem. Commun.*, 2009, 3880.
43 J. J. Shao, W. Lv, Q. Guo, C. Zhang, Q. Xu, Q. H. Yang and F. Kang, *Chem. Commun.*, 2012, **48**, 3706.
44 G. Zhu, Y. Liu, Z. Xu, T. Jiang, C. Zhang, X. Li and G. Qi, *ChemPhysChem*, 2010, **11**, 2432.
45 C. Chen, Q. H. Yang, Y. Yang, W. Lv, Y. Wen, P. X. Hou, M. Wang and H. M. Cheng, *Adv. Mater.*, 2009, **21**, 3007.
46 Z. Ouyang, J. Li, J. Wang, Q. Li, T. Ni, X. Zhang, H. Wang, Q. Li, Z. Su and G. Wei, *J. Mater. Chem. B*, 2013, **1**, 2415.